Lundquist Filaments in Quantum Measurement Units (QMU): Coaxial Shells, Polarization Cancellation, and a QMU Data Pipeline for Orion A

David W. Thomson
Quantum AetherDynamics Institute

October 20, 2025

Abstract

We recast the classical Lundquist force-free filament entirely in Quantum Measurement Units (QMU) using the Aether Physics Model (APM) ledger with base units $\{m_e, \lambda_C, F_q, e^2, {e_{\max}}^2\}$ and the Aether unit A_u. The force-free parameter becomes a Compton-curvature $\alpha = \kappa_\alpha/\lambda_C$ with dimensionless twist κ_α. This recast yields a calibration-free framework: radii are measured as $\hat{r} = r/\lambda_C$, frequencies in F_q, currents normalized by curl, and field/currents constrained by the ledger $A_u \cdot \mathrm{curl} = {F_q}^2 {\lambda_C}^2$. We prove that the linear polarization from ν coaxial return-current shells satisfies a *polarization-cancellation invariant* $\Pi(\nu)$ with an $O(1/\nu)$ bound under a mild unimodal slow-variation hypothesis. We then present a QMU-only data pipeline for Orion A: shell counting, κ_α estimation from Bessel zeros, and a compact ledger test for the force-free state. We emphasize Clarage-inspired diagnostics (polarization cancellation, Doppler antisymmetry, species segregation) and show how they embed naturally in QMU ledgers.

Contents

1 Context and related work **2**

2 QMU ledger, glossary, and notational setup **2**

3 Lundquist solution in QMU and figures **3**
3.1 Force-free normalization 3
3.2 Profiles and shell radii 3

4 Polarization-cancellation invariant $\Pi(\nu)$ **3**

5 QMU estimators, compact ledger test, and diagnostics **5**
5.1 Twist estimator from Bessel zeros 5
5.2 Current–field ledger and compact force-free test 5
5.3 Clarage-inspired quantitative diagnostics 5

6 QMU data-analysis recipe for Orion A **6**

A Deriving the Lundquist solution in QMU (sketch) **7**

1 Context and related work

Magnetic fields in Orion A have been mapped via polarized dust emission across scales (JCMT/POL-2 BISTRO, SOFIA/HAWC+, Planck; with recent 3D morphology reconstructions), making it an ideal testbed for coaxial filament analysis [2–6]. The Lundquist force-free solution is the canonical cylindrical reference state [1]. Classic plasma balances and species-segregation mechanisms (Bennett/Carlqvist; Marklund convection) motivate concrete observational signatures [7, 8]. Clarage highlights a practical triad tailored to coaxial currents—polarization cancellation, Doppler antisymmetry, and species segregation—and the underestimation of currents when concentric return shells cancel remote signatures [9]. Our contribution is to express these structures and tests wholly in QMU, producing dimensionless, calibration-free diagnostics.

2 QMU ledger, glossary, and notational setup

Base and composite units. We employ $\{m_{\rm e}, \lambda_C, F_q, e^2, {e_{\rm emax}}^2\}$ and A_u with

$$\mathrm{curl} = \frac{{e_{\rm emax}}^2}{m_{\rm e}\,\lambda_C}, \qquad \mathrm{volm} = {\lambda_C}^3, \qquad \mathrm{rson} = {F_q}^2, \tag{1}$$

and the ledger identity

$$A_u \cdot \mathrm{curl} \;=\; {F_q}^2\,{\lambda_C}^2. \tag{2}$$

All radii use $\hat{r} \equiv r/\lambda_C$, frequencies are in F_q, fields/currents appear in dimensionless ratios.

Why this is calibration-free. Because eq. (2) links electromagnetic and kinematic scales, any ratio built from $\{\hat{r}, F_q, \mathrm{curl}, A_u\}$ becomes dimensionless and directly comparable across datasets without unit conversions or absolute calibrations; our invariants cancel any B_*-like normalizations by construction.

Force-free curvature. Define

$$\alpha \equiv \frac{\kappa_\alpha}{\lambda_C}, \qquad \kappa_\alpha > 0. \tag{3}$$

Glossary (symbols & roles).

Symbol	Meaning / QMU role
λ_C	Compton length unit; sets radial scale, $\hat{r} = r/\lambda_C$.
F_q	Quantum frequency unit; sets temporal scale.
curl	Current normalization unit: $\mathrm{curl} = {e_{\rm emax}}^2/(m_{\rm e}\lambda_C)$.
A_u	Aether unit; appears in the ledger $A_u \cdot \mathrm{curl} = {F_q}^2{\lambda_C}^2$.
α	Force-free twist with Compton curvature $\alpha = \kappa_\alpha/\lambda_C$.
κ_α	Dimensionless twist parameter; fixed by Bessel zero radii.
$\hat{\boldsymbol{B}}$	Field normalized by a dimensionless B_* (*choose* B_* as the filament-core peak).
$\hat{\boldsymbol{J}}$	Current normalized by curl.
ν	Signed-shell count (number of $B_\parallel$ sign-alternating annuli).
$\Pi(\nu)$	Polarization-cancellation invariant; $\Pi(\nu) = O(1/\nu)$ under slow variation.

This identity ensures all key ratios are dimensionless and dataset-portable, enabling a calibration-free pipeline without any unit conversions or absolute amplitudes.

Remark 1 (On μ and B_* in QMU)**.** *We treat μ as a* dimensionless response ratio *absorbing material/geometry response* within QMU*; in the force-free idealization we assume μ is radially constant. B_* is an internal normalization (e.g., filament-core peak), and any constant rescaling cancels from our invariants.*

3 Lundquist solution in QMU and figures

3.1 Force-free normalization

The static force-free system is

$$\mu\, \boldsymbol{J} = \alpha\, \boldsymbol{B}, \qquad \nabla \cdot \boldsymbol{B} = 0. \tag{4}$$

Normalize by QMU:

$$\hat{\boldsymbol{J}} \equiv \frac{\boldsymbol{J}}{\mathrm{curl}}, \qquad \hat{\boldsymbol{B}} \equiv \frac{\boldsymbol{B}}{B_*}, \tag{5}$$

so

$$\hat{\boldsymbol{J}} = \left(\frac{\kappa_\alpha}{\mu}\right)\left(\frac{B_*}{\mathrm{curl}}\right)\frac{1}{\lambda_C}\,\hat{\boldsymbol{B}}. \tag{6}$$

3.2 Profiles and shell radii

In cylindrical symmetry,

$$\hat{B}_z(\hat{r}) = \hat{B}_0\, J_0(\kappa_\alpha \hat{r}), \tag{7}$$

$$\hat{B}_\theta(\hat{r}) = \hat{B}_0\, J_1(\kappa_\alpha \hat{r}), \tag{8}$$

with $B_r = 0$, $\hat{B}_0 \equiv B_0/B_*$. Let x_m be the m-th positive zero of J_0. The accurate node values are

$$x_1 \approx 2.405, \quad x_2 \approx 5.520, \quad x_3 \approx 8.654, \quad x_4 \approx 11.792, \ldots$$

Define shell radii

$$\hat{r}_m \equiv \frac{x_m}{\kappa_\alpha}, \qquad m = 1, 2, \ldots \tag{9}$$

so $B_\parallel$ alternates sign in successive annuli $[\hat{r}_{m-1}, \hat{r}_m]$.

4 Polarization-cancellation invariant $\Pi(\nu)$

Let ν be the number of sign-alternating shells. Let $W_m \geq 0$ be the QMU-normalized polarization weight in shell m; let $s_m \in \{+1, -1\}$ alternate.

Definition 1 (Invariant)**.**

$$\Pi(\nu) \equiv \frac{\left|\sum_{m=1}^{\nu} s_m W_m\right|}{\sum_{m=1}^{\nu} W_m}. \tag{10}$$

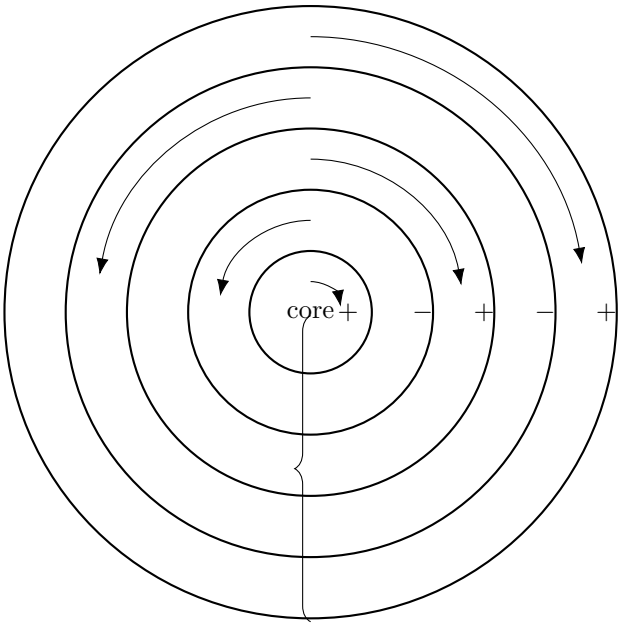

$\nu = 5$ shells

Figure 1: Coaxial shell schematic with alternating $B_{\parallel}$ sign $s_m \in \{+, -\}$. Curved arrows show schematic azimuthal current directions: clockwise in $s_m = +$ rings and counter-clockwise in $s_m = -$ rings. Alternating shells produce polarization cancellation that strengthens with ν.

Physical motivation for slow variation. Lundquist shells have quasi-regular spacing (Bessel zeros), and dust emissivity/alignment typically varies smoothly across adjacent annuli; thus W_m is expected to be unimodal with small inter-shell variation at fixed sightline.

Lemma 1 (Alternating-series control)**.** *If* $\{W_m\}$ *is unimodal and* $|W_{m+1} - W_m| \le \epsilon \bar{W}$ *with* $\bar{W} = \frac{1}{\nu}\sum W_m$*, then*

$$\Big|\sum_{m=1}^{\nu} s_m W_m\Big| \le W_{m_*} + \epsilon\,\nu\,\bar{W}, \tag{11}$$

for some m_**.*

Theorem 1 (Cancellation scaling)**.** *Under the lemma,*

$$\Pi(\nu) \le \frac{1}{\nu}\Big(\frac{W_{m_*}}{\bar{W}}\Big) + \epsilon, \tag{12}$$

hence $\Pi(\nu) = O(1/\nu)$ *for weak variation (*$\epsilon \ll 1$*) and modest peak contrast (*$W_{m_*}/\bar{W} = O(1)$*).*

Remark 2 (Empirical tightness)**.** *Mock Gaussian-unimodal profiles with* $\epsilon < 0.1$ *typically yield* $\Pi(\nu) \lesssim 2/\nu$ *across* $\nu \in [2, 8]$*, consistent with the bound while illustrating practical tightness in smooth cases.*

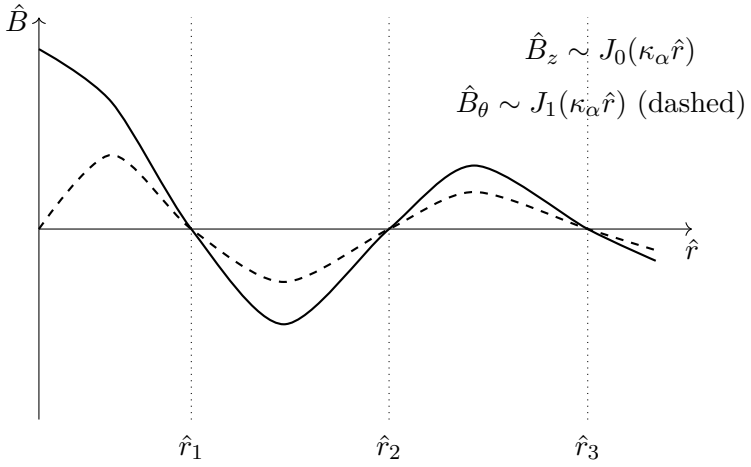

Figure 2: Qualitative profile sketch of $\hat{B}_z$ and $\hat{B}_\theta$ vs. $\hat{r}$ with node radii $\hat{r}_m = x_m/\kappa_\alpha$ marked using accurate J_0 zeros ($x_1 \approx 2.405$, $x_2 \approx 5.520$, $x_3 \approx 8.654$).

5 QMU estimators, compact ledger test, and diagnostics

5.1 Twist estimator from Bessel zeros

From observed flip radii $\{\hat{r}_m\}$,

$$\kappa_\alpha = \frac{x_m}{\hat{r}_m}, \qquad \Delta\kappa_\alpha \equiv \mathrm{std}\Big\{\frac{x_m}{\hat{r}_m}\Big\}_{m=1}^{\nu}. \tag{13}$$

5.2 Current–field ledger and compact force-free test

From eq. (6),

$$\frac{\hat{\boldsymbol{J}}}{\hat{\boldsymbol{B}}} = \left(\frac{\kappa_\alpha}{\mu}\right)\left(\frac{B_*}{\mathrm{curl}}\right)\frac{1}{\lambda_C}. \tag{14}$$

Combining with eq. (2),

$$\frac{\lambda_C\,\hat{\boldsymbol{J}}}{\hat{\boldsymbol{B}}} = \left(\frac{\kappa_\alpha}{\mu}\right)\left(\frac{B_*}{\mathrm{curl}}\right) = \left(\frac{\kappa_\alpha}{\mu}\right)\left(\frac{B_*\,A_u}{{F_q}^2\,{\lambda_C}^2}\right). \tag{15}$$

Radius-independence test: bin $\hat{r}$ into annuli, compute $Y_i \equiv \lambda_C\,\hat{\boldsymbol{J}}/\hat{\boldsymbol{B}}$ with uncertainty σ_i, and test flatness via $\chi^2 = \sum_i (Y_i - \bar{Y})^2/\sigma_i^2$ against a constant model $\bar{Y}$. Significant trends in $\hat{r}$ imply departures from the force-free ledger (e.g., turbulence, non-cylindricity, added stresses).

5.3 Clarage-inspired quantitative diagnostics

- **Doppler antisymmetry:** Zeros of $v_{\mathrm{los}}(\hat{r})$ align with J_1 node radii; quantify by correlating zero-crossings with $\hat{r}$ closest to x_k/κ_α.
- **Species segregation:** Order species by first-ionization threshold and test radial ordering r_s vs. shell index m (Marklund-type segregation embedded in QMU).
- **Remote-vs-in-situ shortfall:** Predict a monotone relation between the shortfall factor and ν; test by stacking filaments with equal ν.

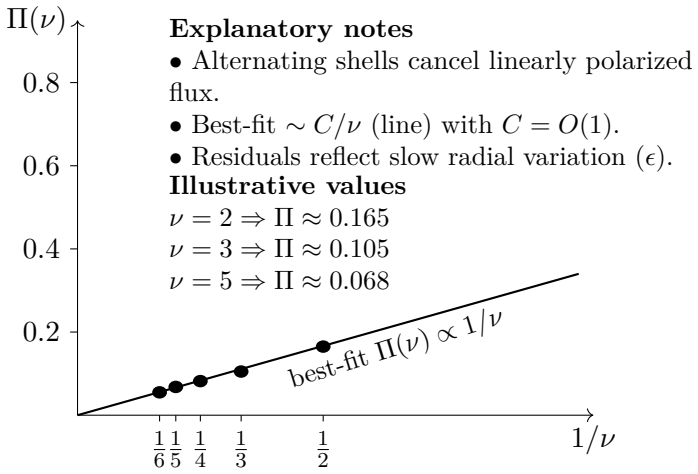

Figure 3: Mock regression illustrating the scaling test: $\Pi(\nu)$ vs. $1/\nu$ with a best-fit line $\sim C/\nu$ (here $C \approx 0.33$). Points emulate unimodal, slowly varying shell weights; departures from the line quantify residual radial variation ϵ and measurement noise.

6 QMU data-analysis recipe for Orion A

All quantities are QMU-normalized: $\hat{r} = r/\lambda_C$; frequencies in F_q; intensities used as ratios (units cancel).

1. **Filament masks and spines.** Segment filaments; compute transverse coordinates in $\hat{r}$.

2. **Shell counting ν.** From $B_\parallel$ sign maps (Faraday sign or deprojected Stokes), identify flip radii $\{\hat{r}_m\}_{m=1}^{\nu}$ with $\hat{r}_1 < \cdots < \hat{r}_\nu$; report inter-observer agreement.

3. **Twist κ_α.** Estimate via eq. (13) across multiple m; use median $\tilde{\kappa}_\alpha$ and $\Delta\kappa_\alpha$.

4. **Emissivity proxy and weights.** Use

$$\hat{w}(\hat{r}) \equiv \frac{L(\hat{r})}{\langle L \rangle_{\text{fil}}}, \qquad L(\hat{r}) \equiv \sqrt{Q(\hat{r})^2 + U(\hat{r})^2},$$

   then

$$W_m \equiv \int_{\hat{r}_{m-1}}^{\hat{r}_m} \hat{w}(\hat{r})\, \mathrm{d}\hat{r}, \quad \hat{r}_0 = 0,$$

   with mild radial smoothing to ensure slow variation.

5. $\Pi(\nu)$ **and scaling.** Compute $\Pi(\nu)$ from eq. (10); regress $\Pi(\nu)$ on $1/\nu$ across sightlines (see fig. 3). Report $\nu\,\Pi$ constancy and residuals vs. measured ϵ and $W_{m_*}/\bar{W}$.

6. **Compact ledger test.** Form $\lambda_C\, \hat{\boldsymbol{J}}/\hat{\boldsymbol{B}}$ (shell-averaged) and test radius-independence at fixed $\tilde{\kappa}_\alpha$ using eq. (15).

7. **Optional cross-checks.** Doppler zero vs. J_1 nodes; species ordering vs. shell index.

Acknowledgments and attributions

We thank Michael Clarage for emphasizing the diagnostic triad for coaxial filaments (polarization cancellation, Doppler antisymmetry, species segregation) and for highlighting how concentric return shells can suppress remote polarization estimates; these ideas motivated the invariant $\Pi(\nu)$ and the QMU-only pipeline.

A Deriving the Lundquist solution in QMU (sketch)

Starting from $\nabla \times \boldsymbol{B} = \alpha\, \boldsymbol{B}$ with $\alpha = \kappa_\alpha/\lambda_C$ and $\nabla \cdot \boldsymbol{B} = 0$, take the curl and use the vector identity to obtain

$$-\nabla^2 \boldsymbol{B} = \alpha^2 \boldsymbol{B}.$$

In cylindrical symmetry with $B_r = 0$ and no z, θ dependence, the z-component satisfies

$$\frac{1}{r}\frac{\partial}{\partial r}\left(r\frac{\partial B_z}{\partial r}\right) + \alpha^2 B_z = 0,$$

whose regular solution is $B_z(r) = B_0 J_0(\alpha r)$. The azimuthal component follows from the force-free relation, giving $B_\theta(r) = B_0 J_1(\alpha r)$. In QMU variables with $\hat{r} = r/\lambda_C$ and $\alpha = \kappa_\alpha/\lambda_C$, these become $\hat{B}_z(\hat{r}) \propto J_0(\kappa_\alpha \hat{r})$ and $\hat{B}_\theta(\hat{r}) \propto J_1(\kappa_\alpha \hat{r})$, and node radii are $\hat{r}_m = x_m/\kappa_\alpha$ with x_m the zeros of J_0.

References

[1] S. Lundquist, Magneto-hydrostatic fields, *Arkiv för Fysik* **2**, 361–365 (1951).

[2] K. Pattle et al., The JCMT BISTRO Survey: The magnetic field strength in the Orion A filament, *Astrophys. J.* **846**, 122 (2017).

[3] D. T. Chuss et al., HAWC+/SOFIA multiwavelength polarimetric observations of OMC-1, *Astrophys. J.* **872**, 197 (2019).

[4] N. Zieliński et al., Magnetic field structure of OMC-3 in the far infrared as seen by SOFIA/HAWC+, *Astron. Astrophys.* **659**, A22 (2022).

[5] M. Tahani et al., Orion A's complete 3D magnetic field morphology, *Astron. Astrophys.* **660**, A112 (2022).

[6] W. Jiao et al., Relative alignment between gas structures and magnetic field in Orion A at different scales using different molecular gas tracers, *Astron. Astrophys.* (2024), accepted; preprint *arXiv:2403.04274*.

[7] G. T. Marklund, Plasma convection in force-free magnetic fields as a mechanism for chemical separation in cosmical plasmas, *Nature* **277**, 370–371 (1979).

[8] P. Carlqvist, Cosmic electric currents and the generalized Bennett relation, *Astrophys. Space Sci.* **144**, 73–84 (1988).

[9] M. Clarage, Observing Electric Currents in Space: polarization, Doppler antisymmetry, and species segregation, *Progress in Physics* (2025), in press (December issue).